Chapter 21

Equatorial Dynamics

ABSTRACT
Because the Coriolis force vanishes along the equator, tropical regions exhibit particular dynamics. After an overview of linear waves that exist only along the equator, the chapter concludes with a brief presentation of the episodic transfer of warm waters from the western to the eastern tropical Pacific Ocean, a phenomenon called El Niño. The problem of its seasonal forecast then allows us to introduce another type of predictive tool, one based on empirical relationships.

21.1 EQUATORIAL BETA PLANE

Along the equator (latitude $\varphi = 0°$), the Coriolis parameter $f = 2\Omega \sin\varphi$ vanishes. Without a horizontal Coriolis force, currents cannot be maintained in geostrophic balance, and we expect dramatic dynamical differences between tropical and extratropical regions. The first question is the determination of the meridional extent of the tropical region where these special effects can be expected.

It is most natural here to choose the equator as the origin of the meridional axis. The beta-plane approximation to the Coriolis parameter (see Section 9.4) then yields

$$f = \beta_0 y, \tag{21.1}$$

where y measures the meridional distance from the equator (positive northward) and $\beta_0 = 2\Omega/a = 2.28 \times 10^{-11}\,\mathrm{m^{-1}\,s^{-1}}$ with Ω and a being, respectively, the earth's angular rotation rate and radius ($\Omega = 7.29 \times 10^{-5}\,\mathrm{s^{-1}}$, $a = 6371\,\mathrm{km}$). This representation of the Coriolis parameter bears the name of *equatorial beta-plane* approximation.

Our previous considerations of midlatitude processes (see Chapter 16, for example) point to the important role played by the internal deformation radius,

$$R = \frac{\sqrt{g'H}}{f} = \frac{c}{f}, \tag{21.2}$$

Introduction to Geophysical Fluid Dynamics, Volume 101, ISSN 0074-6142, DOI: 10.1016/B978-0-12-088759-0.00021-3

in governing the extent of dynamical structures. Here, g' is a suitable reduced gravity characterizing the stratification and H is a layer thickness. As f varies with y, so does R. If this distance from a given meridional position y includes the equator, equatorial dynamics must supersede midlatitude dynamics. Thus, a criterion to determine the width R_{eq} of the tropical region is (Fig. 21.1)

$$R_{eq} = R \quad \text{at} \quad y = R_{eq}. \tag{21.3}$$

Substituting Eq. (21.1) in Eq. (21.2), the criterion yields

$$R_{eq} = \sqrt{\frac{c}{\beta_0}}, \tag{21.4}$$

which is called the *equatorial radius of deformation*. For the previously quoted value of β_0 and for $c = (g'H)^{1/2} = 1.4$ m/s, typical of the tropical ocean (Philander, 1990, Chapter 3), we estimate $R_{eq} = 248$ km, or 2.23° of latitude. Because the stratification of the atmosphere is much stronger than that of the ocean, the equatorial radius of deformation is several times larger in the atmosphere. This implies that connections between tropical and temperate latitudes are different in the atmosphere and oceans.

Since c is a velocity (to be related shortly to a wave speed), we can define an *equatorial inertial time* T_{eq} as the travel time to cover the distance R_{eq} at speed c. Simple algebra yields

$$T_{eq} = \frac{1}{\sqrt{\beta_0 c}}, \tag{21.5}$$

which, for the previous values, is about 2 days.

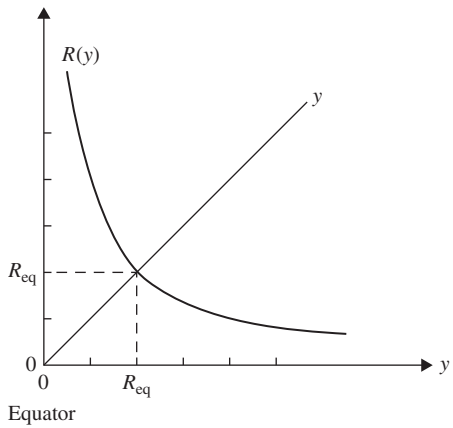

FIGURE 21.1 Definition of the equatorial radius of deformation.

21.2 LINEAR WAVE THEORY

Because of the important role they play in the so-called El Niño phenomenon, the focus of this section is on oceanic waves. The stratification of the equatorial ocean generally consists of a distinct warm layer separated from the deeper waters by a shallow thermocline (Fig. 21.2). Typical values are $\Delta\rho/\rho_0 = 0.002$ and thermocline depth $H = 100\,\text{m}$, leading to the previously quoted value of $c = (g'H)^{1/2} = 1.4\,\text{m/s}$. This suggests the use of a one-layer reduced-gravity model, which for the purpose of a wave theory is immediately linearized:

$$\frac{\partial u}{\partial t} - \beta_0 y\, v = -g' \frac{\partial h}{\partial x} \tag{21.6a}$$

$$\frac{\partial v}{\partial t} + \beta_0 y\, u = -g' \frac{\partial h}{\partial y} \tag{21.6b}$$

$$\frac{\partial h}{\partial t} + H\left(\frac{\partial u}{\partial x} + \frac{\partial v}{\partial y}\right) = 0. \tag{21.6c}$$

Here u and v are, respectively, the zonal and meridional velocity components, g' the reduced gravity $g\Delta\rho/\rho_0$ ($= 0.02\,\text{m/s}^2$), and h the layer thickness variation (thickening counted positively and thinning counted negatively).

The preceding set of equations admits a solution with zero meridional flow. When $v = 0$, Eqs. (21.6a) and (21.6c) reduce to

$$\frac{\partial u}{\partial t} = -g'\frac{\partial h}{\partial x}, \qquad \frac{\partial h}{\partial t} + H\frac{\partial u}{\partial x} = 0,$$

having any function of $x \pm ct$ and y as its solution. The remaining equation, (21.6b), sets the meridional structure, which for a signal decaying away from

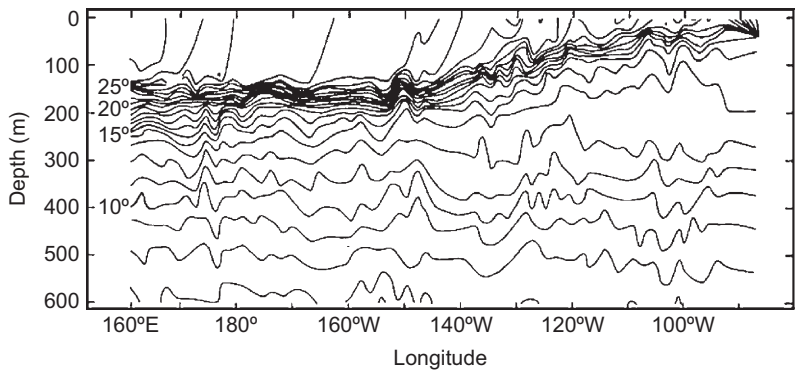

FIGURE 21.2 Temperature (in °C) as a function of depth and longitude along the equator, as measured in 1963 by Colin, Henin, Hisard and Oudot (1971). Note the strong thermocline between 100 and 200 m.

the equator is given by

$$u = cF(x-ct)\mathrm{e}^{-y^2/2R_{\mathrm{eq}}^2} \tag{21.7a}$$

$$v = 0 \tag{21.7b}$$

$$h = HF(x-ct)\mathrm{e}^{-y^2/2R_{\mathrm{eq}}^2}, \tag{21.7c}$$

where $F(\cdot)$ is an arbitrary function of its argument and $R_{\mathrm{eq}} = (c/\beta_0)^{1/2}$ is the equatorial radius of deformation introduced in the preceding section. This solution describes a wave traveling eastward at speed $c = \sqrt{g'H}$, with maximum amplitude along the equator and decaying symmetrically with latitude over a distance on the order of the equatorial radius of deformation. The analogy with the coastal Kelvin wave exposed in Section 9.2 is immediate: wave speed equal to gravitational wave speed, absence of transverse flow, nondispersive behavior, and decay over a deformation radius. For this reason, it is called the *equatorial Kelvin wave*. Credit for the discovery of this wave, however, does not go to Lord Kelvin but to Wallace and Kousky (1968).

The set of equations (21.6) admits additional wave solutions, more akin to inertia-gravity (Poincaré) and planetary (Rossby) waves. To find these, we seek periodic solutions in time and zonal direction:

$$u = U(y)\cos(kx-\omega t) \tag{21.8a}$$

$$v = V(y)\sin(kx-\omega t) \tag{21.8b}$$

$$h = A(y)\cos(kx-\omega t). \tag{21.8c}$$

Elimination of the $U(y)$ and $A(y)$ amplitude functions yields a single equation governing the meridional structure $V(y)$ of the meridional velocity:

$$\frac{\mathrm{d}^2V}{\mathrm{d}y^2} + \left(\frac{\omega^2-\beta_0^2y^2}{c^2} - \frac{\beta_0 k}{\omega} - k^2\right)V = 0. \tag{21.9}$$

Because the expression between parentheses depends on the variable y, the solutions to this equation are not sinusoidal. In fact, for values of y sufficiently large, this coefficient becomes negative, and we anticipate exponential decay at large distances from the equator. It can be shown that solutions of Eq. (21.9) are of the type

$$V(y) = H_n\left(\frac{y}{R_{\mathrm{eq}}}\right)\mathrm{e}^{-y^2/2R_{\mathrm{eq}}^2}, \tag{21.10}$$

where H_n is a polynomial of degree n, and that solutions decaying at large distances from the equator exist only if

$$\frac{\omega^2}{c^2} - k^2 - \frac{\beta_0 k}{\omega} = \frac{2n+1}{R_{\mathrm{eq}}^2}. \tag{21.11}$$

Thus, the waves form a discrete set of modes ($n = 0, 1, 2, \ldots$). Equation (21.11) is the dispersion relation providing frequencies ω as a function of wavenumber k for each mode. As Fig. 21.3 shows, three ω roots exist for each n as k varies. (Important note: In this context, the phase speed ω/k of the wave is not necessarily equal to c, the speed of the Kelvin wave encountered previously.)

The largest positive and negative roots for $n \geq 1$ correspond to frequencies greater than the inverse of the equatorial inertial time. The slight asymmetry in these curves is caused by the beta term in Eq. (21.11). Without this term, the frequencies can be approximated by

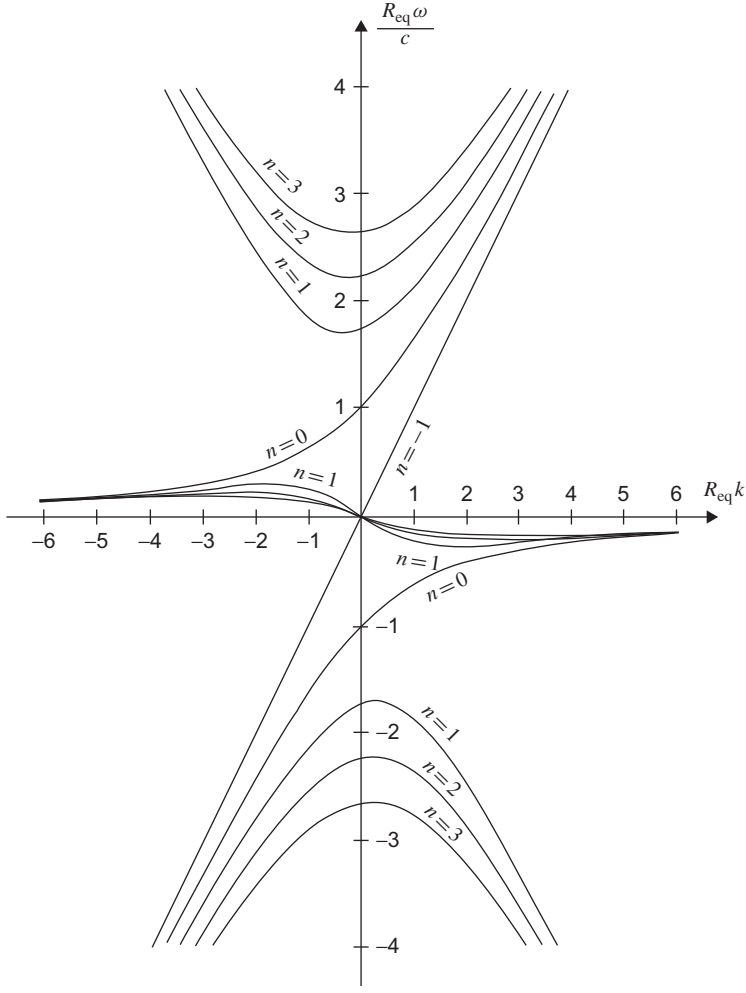

FIGURE 21.3 Dispersion diagram for equatorially trapped waves.

$$\omega \simeq \pm \sqrt{\frac{2n+1}{T_{\text{eq}}^2} + g'Hk^2}, \qquad n \geq 1, \tag{21.12}$$

which is analogous to Eq. (9.17), the dispersion relation of inertia-gravity waves. These waves are thus the low-latitude extensions of the extratropical inertia-gravity waves (Section 9.3).

The third and much smaller roots for $n \geq 1$ correspond to subinertial frequencies and thus to tropical extensions of the midlatitude planetary waves (Section 9.4). At long wavelengths (small k values), these waves are nearly nondispersive and propagate westward at speeds

$$c_n = \frac{\omega_n}{k} \simeq -\frac{\beta_0 R_{\text{eq}}^2}{2n+1}, \qquad n \geq 1, \tag{21.13}$$

which are to be compared with Eq. (9.30).

The case $n = 0$ is peculiar. Its frequency ω_0 is the root of

$$(\omega_0 + ck)\left(\omega_0 T_{\text{eq}} - \frac{1}{\omega_0 T_{\text{eq}}} - kR_{\text{eq}}\right) = 0. \tag{21.14}$$

The root $\omega_0 = -ck$ can be shown to be a spurious solution introduced during the elimination of $U(y)$ from the governing equation. This elimination indeed assumed $\omega_0 + ck \neq 0$, which we therefore may not accept as a valid solution. The remaining two roots are readily calculated. As Fig. 21.3 shows, this wave exhibits a mixed behavior between planetary and inertia-gravity waves. Finally, the Kelvin-wave solution can formally be included in the set by taking $n = -1$ (Fig. 21.3).

The polynomials of Eq. (21.10) are not arbitrary but must be the so-called Hermite polynomials (Abramowitz & Stegun, 1972, Chapter 22). The first few polynomials of this set are $H_0(\xi) = 1$, $H_1(\xi) = 2\xi$ and $H_2(\xi) = 4\xi^2 - 2$. From the solution $V(y)$, the layer thickness anomaly $A(y)$ can be retrieved by backward substitution. It is seen that when V is odd in y, A is even, and vice versa. Waves of even order are antisymmetric about the equator $[h(-y) = -h(y)]$, whereas those of odd order are symmetric $[h(-y) = h(y)]$. The mixed wave is antisymmetric and the Kelvin wave is symmetric.

When the equatorial ocean is perturbed (e.g., by changing winds), its adjustment toward a new state is accomplished by wave propagation. At low frequencies (periods longer than T_{eq}, or about 2 days), inertia-gravity waves are not excited, and the ocean's response consists entirely of the Kelvin wave, the mixed wave, and some planetary waves (those of appropriate frequencies). If, moreover, the perturbation is symmetric about the equator (and generally there is a high degree of symmetry about the equator), the mixed wave and all planetary waves of even order are ruled out. The Kelvin wave and odd planetary waves of short wavelengths (if any) carry energy eastward, whereas the odd planetary waves of long wavelengths carry energy westward. Figure 21.4 displays the

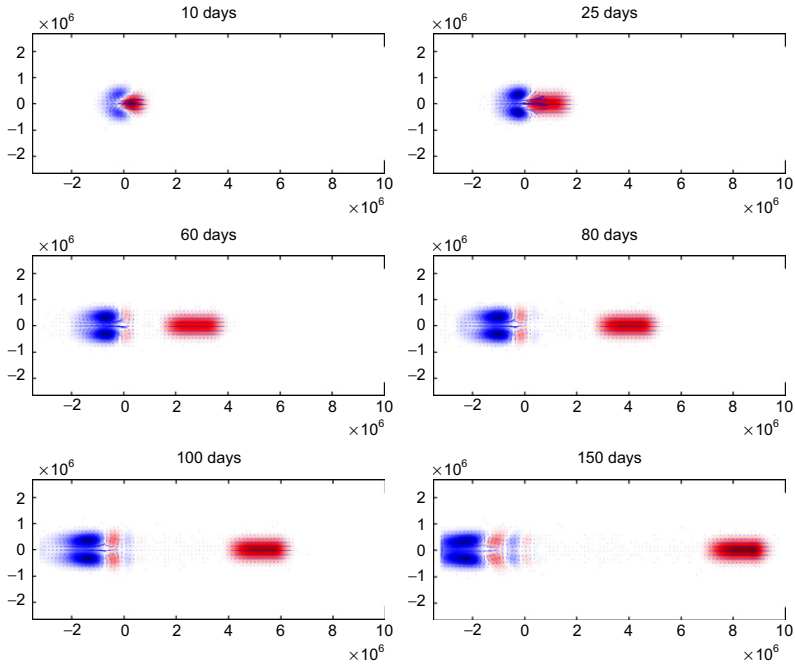

FIGURE 21.4 The dispersion of a perturbation generated by a 10-day wind anomaly imposed on a spot of the equatorial ocean. Clearly visible are the one-bulge Kelvin wave moving eastward and the double-bulge planetary (Rossby) wave propagating westward at a slower pace.

temporal dispersion of a thermocline displacement generated by a wind-stress anomaly imposed on a stretch of equatorial ocean. Clearly visible are the one-bulge Kelvin wave progressing eastward and the double-bulge lowest planetary wave ($n = 1$) propagating westward. Although this case is obviously academic, it is believed that Kelvin waves and low-order planetary waves, together with wind-driven currents, are frequent in the equatorial ocean.

At this point, a number of interesting topics can be presented, such as the reflection of a Kelvin wave upon encountering an eastern boundary (Fig. 21.5), waves around islands, and the generation of equatorial currents by time-dependent winds. We shall, however, leave these matters for the more specialized literature (Gill, 1982; Philander, 1990; McPhaden & Ripa, 1990; and references therein) and limit ourselves to the presentation of the El Niño phenomenon.

21.3 EL NIÑO – SOUTHERN OSCILLATION (ENSO)

Every year, around the Christmas season, warm waters flow along the western coast of South America from the equator to Peru and beyond. These

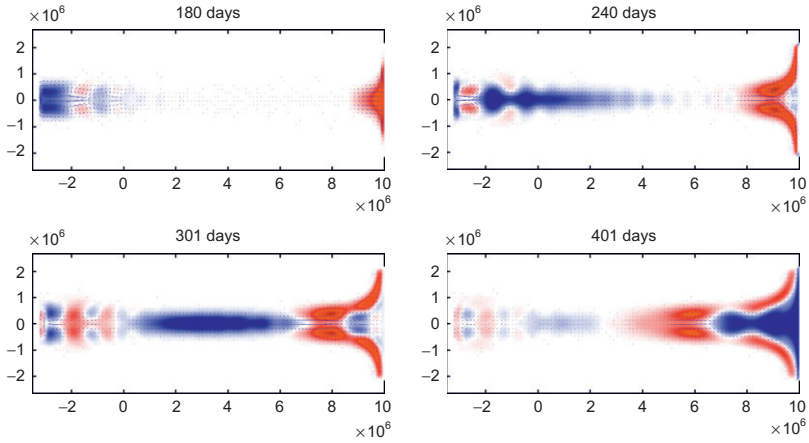

FIGURE 21.5 Continuation of the wave propagation shown in the preceding figure. Planetary (Rossby) waves are reflected at the western wall and turned into Kelvin waves, while the Kelvin wave generates a planetary wave after reflection against the eastern boundary.

waters, which are several degrees warmer than usual and are much less saline, perturb the coastal ocean, suppressing—among other things—the semipermanent coastal upwelling of cold waters. So noticeable is this phenomenon that early fishermen called it El Niño, which in Spanish means "the child" or more specifically the Christ Child, in relation to the Christmas season.

Regularly but not periodically (every 3 to 7 years), the amount of passing warm waters is substantially greater than in normal years, and life in those regions is greatly perturbed, for better and for worse. Anomalously abundant precipitations, caused by the warm ocean, can in a few weeks turn the otherwise arid coastal region of Peru into a land of plenty. But, suppression of coastal upwelling causes widespread destruction of plankton and fish. The ecological and economic consequences are noticeable. In Peru, the fish harvest is much reduced, sea birds (which prey on fish) die in large numbers, and, to compound the problem, dead fish and birds rotting on the beach create unsanitary atmospheric conditions.

In the scientific community, the name El Niño is being restricted to such anomalous occurrences and, by extension, the name La Niña has been used to signify the opposite situation, when waters are abnormally cold in the eastern tropical Pacific. Major El Niño events of the twentieth century occurred in 1904–05, 1913–15, 1925–26, 1940–41, 1957–58, 1972–73, 1982–83, 1986–88, 1991–95, 1997–98 (the strongest of all), and sofar in twenty-first century in 2002–2003, 2004–2005, and 2006–2007 (WMO, 1999; NOAA-WWW, 2006). Their cause remained obscure until Wyrtki (1973) discovered a strong correlation with changes in the central and western tropical Pacific Ocean, thousands of

kilometers away. It is now well established (Philander, 1990) that El Niño events are caused by changes in the surface winds over the tropical Pacific, which episodically release and drive warm waters, previously piled up by trade winds in the western half of the basin, eastward to the American continent and southward along the coast. The situation is quite complex, and it took oceanographers and meteorologists more than a decade to understand the various oceanic and atmospheric factors.

Under normal conditions, winds over the tropical Pacific Ocean consist of the northeast trade winds (northeasterlies) and the southeast trade winds (southeasterlies) that converge over the *intertropical convergence zone* (ITCZ) and blow westward (Section 19.3). Although it migrates meridionally in the course of the year, the ITCZ sits predominantly in the northern hemisphere (around 5° to 10°N). In addition to pushing and accumulating warm water in the western tropical Pacific, the trade winds also generate equatorial upwelling (Section 15.4) over the eastern part of the basin. Thus, in a normal situation, the tropical Pacific Ocean is characterized by a warm water pool in the west and cold surface waters in the east. This structure is manifested by the westward deepening of the thermocline, as shown in Fig. 21.2.

The origin of an anomalous, El Niño event is associated with a weakening of the trade winds in the western Pacific or with the appearance of a warm sea surface temperature (SST) anomaly in the central tropical Pacific. Although one may precede the other, they soon go hand in hand. A slackening of the western trades relaxes the thermocline slope and releases some of the warm waters; this relaxation takes the form of a downwelling Kelvin wave, whose wake is thus a warm SST anomaly. On the other hand, a warm SST anomaly locally heats the atmosphere, creating ascending motions that need to be compensated by horizontal convergence. This horizontal convergence naturally calls for eastward winds on its western side, thus weakening or reversing the trade winds there (Gill, 1980). In sum, a relaxation of the trade winds in the western Pacific creates a warm sea surface anomaly, and vice versa. Feedback occurs and the perturbation amplifies. On the eastern side of the anomaly, convergence calls for a strengthening of the trades that, in turn, enhances equatorial upwelling. This cooling interferes with the eastward progression of the downwelling Kelvin wave, and it is not clear which should dominate. During an El Niño event, the anomaly does travel eastward while amplifying. Once the warm water arrives at the American continent, it separates into a weaker northward branch and a stronger southward branch, each becoming a coastal Kelvin wave (downwelling). The subsequent events are as described at the beginning of this section.

When an El Niño event occurs, its temporal development is strictly controlled by the annual cycle. The warm waters arrive in Peru around December, and the seasonal variation of the general atmospheric circulation calls for a northward return of the ITCZ and a reestablishment of the southeast trade winds along the equator. The situation returns to normal.

This sequence of events is relatively well understood (Philander, 1990) and has been successfully modeled (Cane, Zebiak & Dolan, 1986). Today, models are routinely used to forecast the next occurrence of an El Niño event and its intensity with a lead time of 9 to 12 months. What remains less clear is the variability of the atmosphere-ocean system on the scales of several years. A strong connection with the *Southern Oscillation* has been made clear, and the broader phenomenon is called ENSO, for El Niño–Southern Oscillation (Rasmusson & Carpenter, 1982). The Southern Oscillation is a quasi-periodic variation of the surface atmospheric pressure and precipitation distributions over large portions of the globe (Bromwich et al., 2000; Troup, 1965).

Much hinges on variations of the so-called *Walker circulation*. This atmospheric circulation (Walker, 1924) consists of easterly trade winds over the tropical Pacific Ocean, low pressure and rising air above the western basin and Indonesia (with associated heavy precipitation) and, at the eastern end of the basin, high pressure, sinking air, and relatively dry climate. The strength of this circulation is effectively measured by the sea-level pressure difference Δp_{TD} between Tahiti (18°S, 149°W) and Darwin (in northern Australia, at 12°S, 131°E). In practice, the *Southern Oscillation Index* (SOI) is defined as (Troup, 1965):

$$SOI = 10\,\frac{\text{monthly value of } \Delta p_{\mathrm{TD}} - \text{long-term average of } \Delta p_{\mathrm{TD}}}{\text{standard deviation of } \Delta p_{\mathrm{TD}}}, \qquad (21.15)$$

The nearly perfect negative correlation between these two pressures indicates that both are parts of a larger coherent system. The presence of a higher than normal pressure in Darwin with simultaneous lower pressure in Tahiti (negative *SOI* value) is intimately connected with an El Niño occurrence (Fig. 21.6). In its broad lines, the scenario unfolds as follows. A negative SOI value leads to a weakening of the Walker circulation, reduced strength of the easterly trade winds, especially in the western Pacific. The western warm water pool relaxes and begins to spill eastward as an equatorial Kelvin wave toward the central basin, accompanied by a similarly eastward displacement of the low atmospheric pressure above it. Feeding the low pressure from the west, anomalous westerly winds accelerate the eastward movement of the warm water pool. And so, the situation progresses eastward in an amplifying manner until the warm water pool reaches the coast of Peru and an El Niño event occurs. Because atmospheric pressure is then higher than normal on the western side, drought conditions occur over Indonesia and Australia, while South America experiences stronger precipitation than normal. For a more complete description of the many facets and ramifications of the event, the interested reader is referred to specialized books (D'Aleo, 2002; Diaz & Markgraf, 2000; Philander, 1990).

A conceptual model of the ENSO event that captures its major characteristics with a minimum of variables is the so-called recharge-discharge oscillator proposed by Jin (1997a,b). The situation being considered is defined by anomalies with respect to a mean climatological state, the latter being characterized by the Walker circulation, upwelling in the eastern Pacific, and warm water piled

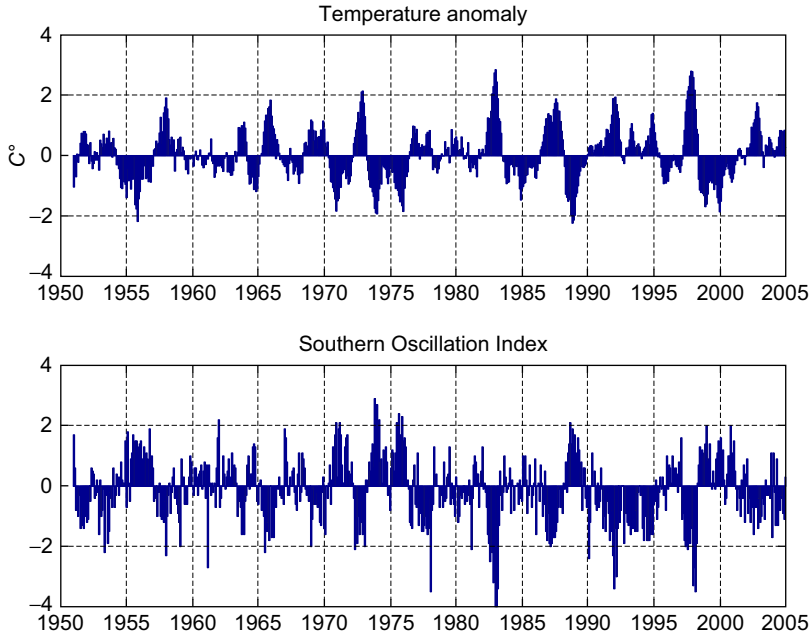

FIGURE 21.6 Time series of temperature anomalies over the central tropical Pacific Ocean and of the Southern Oscillation Index (3-month running means). There is a very strong correlation between higher than normal temperatures (El Niño events) and negative index values, indicating that El Niño is part of a global climatic variation. A spectral analysis of the temporal evolution of SOI reveals a peak in the interval of 3.5–4.5 years. (*NOAA, U.S. Department of Commerce, Washington, D.C.*)

up in the western Pacific. The variables are therefore the anomalies of the wind stress (positive for a westerly anomaly, corresponding to a weakening of the Walker circulation), of the oceanic surface layer thickness (positive for a thicker layer), and of the sea surface temperature (positive at the coast of Peru during an El-Niño event). The oceanic component is modeled as a single, reduced-gravity layer of average depth H. The model distinguishes two depth anomalies, one in the western basin and the other in the eastern basin of the Pacific, one value for each basin without further specification of the zonal and meridional structure. Since El Niño and La Niña are characterized, respectively, by positive and negative temperature anomalies in the eastern Pacific, we limit the temperature description to this anomaly (Fig. 21.7). With these few variables, we now proceed to model the key dynamics.

21.3.1 The Ocean

- *Dynamics*: Under changing wind stress, the ocean adjusts by means of wave propagation, but we may consider the time needed for such an adjustment to be short compared with the seasonal and longer time scales of an ENSO

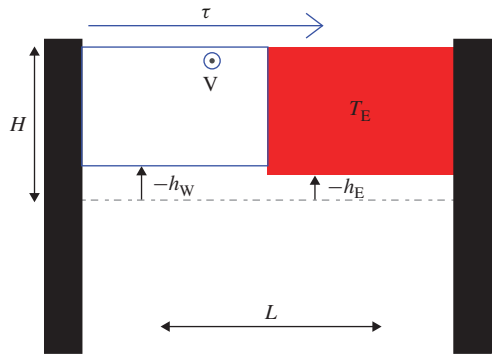

FIGURE 21.7 Schematic situation for a simple ENSO model. Two depth anomalies h_W and h_E are assigned respectively to the western and eastern Pacific basins and are counted positive downward. The water pool in the eastern Pacific, at temperature T_E, can become warmer or colder as a result of an anomaly. A wind blows above the surface, and τ denotes its windstress anomaly, which is responsible for a lateral transport V.

event. Therefore, following Jin (1997a), we suppose that a wind-stress anomaly τ in the zonal direction is instantaneously accompanied by an anomalous pressure difference between eastern and western basins. In the framework of a reduced-gravity model, the pressure-gradient anomaly is expressed as the difference in thermocline depth between East (h_E) and West (h_W), and equilibrium requires

$$g' \frac{h_E - h_W}{L} = \frac{\tau}{\rho_0 H}. \tag{21.16}$$

For a given wind-stress anomaly, we can therefore calculate one of the two depth anomalies from the other. Volume conservation will be the means by which we can write a second relation between the two depth anomalies.

We further assume that the zonal velocity is proportional to the wind-stress anomaly:

$$U = \gamma \tau, \tag{21.17}$$

in which U is the scale that provides the size of the zonal velocity anomaly and γ is an empirical coefficient of proportionality. This is justified for a wind stress that acts over an elongated nonrotating basin (e.g., Mathieu, Deleersnijder, Cushman-Roisin, Beckers & Bolding, 2002), like an equatorial strip.

- *Volume conservation*: During an ENSO event, the temperature anomaly is concentrated in the eastern Pacific, with the wind-stress anomaly occurring on its western flank. The volume budget is first established by integrating volume conservation Eq. (12.9) over the western pool, starting from no flow

at the western boundary. Because of the balance of forces (21.16) in the zonal direction, there is no reason for persisting zonal transport between the western and eastern basins, and this leaves the meridional transport as the only way to export or import waters. Since the depth anomaly is characteristic of the equatorial strip of ocean water, we need to calculate the transport at the northern and southern limits of the equatorial band of interest, which we take as one equatorial radius of deformation from either side of the equator: $y = \pm R_{\text{eq}}$, with R_{eq} defined in Eq. (21.4). According to Eq. (20.11c), a meridional Sverdrup and Ekman transport must exist. With the wind anomaly aligned with the equator, the meridional transport is

$$\mathrm{V} = -\frac{1}{\rho_0 \beta_0} \frac{\partial \tau^x}{\partial y}. \tag{21.18}$$

With atmospheric and oceanic anomalies tightly coupled, we may assume they are both concentrated around the equator in a strip of width $2R_{\text{eq}}$ and that the wind-stress anomaly decreases from τ at the equator to 0 at $y \sim \pm R_{\text{eq}}$, and we estimate

$$\mathrm{V} \approx \pm \frac{1}{\rho_0 \beta_0} \frac{\tau}{R_{\text{eq}}}, \tag{21.19}$$

with the plus (minus) sign at the northern (southern) boundary. It follows that the flow divergence D between the two boundaries is

$$D \approx \frac{\tau}{\rho_0 \beta_0 R_{\text{eq}}^2}. \tag{21.20}$$

This divergence of flow in turn modifies the thermocline depth in the western basin, and the equation governing this thermocline depth is therefore

$$\frac{\mathrm{d}h_W}{\mathrm{d}t} = -D - r h_{\mathrm{W}}, \tag{21.21}$$

where the last term on the right-hand side is intended to represent some damping of the ocean adjustment by lateral mixing and boundary-layer exchange.

- *Heat budget*: When the surface layer is modeled as a reduced-gravity model, a temperature anomaly is susceptible to modify the value of g' but not significantly. In the absence of anomalies, the heat budget of either basin is considered closed, and thus any departure from this unperturbed state is a function of the anomalies only. There are two ways by which the temperature in the eastern basin can be affected, either by zonal advection or by vertical advection.

  The zonal velocity anomaly u caused by the wind-stress anomaly τ moves the background climatological temperature field in or out of the

eastern basin,[1] and we may write

$$u\,\frac{\partial \bar{T}}{\partial x} \sim U\frac{T_{\mathrm{E}}-T_{\mathrm{W}}}{L}, \tag{21.22}$$

in which U is the previously defined scale for the zonal velocity anomaly and related to the wind-stress anomaly τ by Eq. (21.17), and T_{E} and T_{W} are the climatological temperatures in the eastern and western basins, respectively. For positive U (eastward flow under positive wind-stress anomaly τ), the temperature T_{E} in the east increases by import of warmer water from the western pool (because $T_{\mathrm{W}} > T_{\mathrm{E}}$).

For vertical advection, the situation is more subtle. Without anomaly, vertical advection of temperature in the eastern pool is

$$\bar{w}\frac{\partial \bar{T}}{\partial z} \sim \bar{w}\,\frac{\bar{T}_{\mathrm{surf}}-\bar{T}_{-H}}{H}, \tag{21.23}$$

where the overbar refers to the climatological basic state. The strength of the upwelling $\bar{w}$ is proportional to the wind stress, $\bar{w}=-\alpha\bar{\tau}$, with the minus sign corresponding to upwelling under normal easterly trade winds.

A positive wind-stress anomaly τ reduces the upwelling intensity and thus creates a negative upwelling anomaly $\tilde{w}$. Therefore, less deep (and less cold) waters than usual are brought to the surface, and this corresponds to a positive heat flux anomaly. This flux anomaly can be estimated as the difference of Eq. (21.23) in which $\bar{w}$ is replaced by $\bar{w}+\tilde{w}$, and the climatological basic-state equation (21.23):

$$\tilde{w}\frac{T_{\mathrm{surf}}-T_{-H}}{H} \sim -\alpha\tau\,\frac{\Delta_v T}{H}, \tag{21.24}$$

in which $\Delta_v T$ is the vertical temperature difference between climatological surface water and deep water.

If the eastern Pacific has a positive depth anomaly, the temperature at $y=-H$ is not the climatological value, but the climatological value found at $-H+h_{\mathrm{E}}$, because a positive depth anomaly shifts the temperature profile downward. The surface temperature is the surface temperature augmented by the temperature anomaly, and taking the difference of Eq. (21.23) with these two modified temperature values and the reference (21.23) provides

$$-\bar{w}\left(\frac{T_{\mathrm{E}}}{H}-\frac{\partial \bar{T}}{\partial z}\,\frac{h_{\mathrm{E}}}{H}\right) \sim -\frac{\bar{w}}{H}T_{\mathrm{E}}+\frac{\bar{w}\Delta_v T}{H^2}h_{\mathrm{E}}, \tag{21.25}$$

in which we linearized $\bar{T}_{-H+h_{\mathrm{E}}}$ around $\bar{T}_{-H}$. The interpretation of the sign in the term proportional to h_{E} is that a deeper thermocline results in an

[1] Even if the vertically averaged velocity is zero between the western and eastern pools, a wind-induced surface current can displace temperature anomalies.

upwelling of warmer waters than usual, creating a positive temperature anomaly.

Grouping the three contributions into the budget for temperature anomaly, we obtain

$$\frac{\mathrm{d}T_\mathrm{E}}{\mathrm{d}t} = -\left(r' + \frac{\bar{w}}{H}\right) T_\mathrm{E} + \frac{\bar{w}\Delta_v T}{H^2}\, h_\mathrm{E} + \left(\gamma \frac{\Delta_h T}{L} + \alpha \frac{\Delta_v T}{H}\right)\tau, \qquad (21.26)$$

in which $\Delta_h T = T_\mathrm{W} - T_\mathrm{E}$ is the positive climatological temperature difference between western and eastern Pacific. In the first term on the right-hand side, we added a damping effect as for h_W and also included damping by exchanges with the atmosphere.

21.3.2 The Atmosphere

Because of the much lower inertia of the atmosphere compared with the ocean, we may assume that the sea surface anomaly in the east immediately creates a Walker circulation and write

$$\tau = \mu T_\mathrm{E}. \qquad (21.27)$$

The coupling parameter can be calculated by a simplified atmospheric model (Gill, 1980).

21.3.3 The Coupled Model

Gathering the different pieces, we finally obtain the governing equations of the simplified model of an ENSO event:

$$\frac{\mathrm{d}h_\mathrm{W}}{\mathrm{d}t} = -\frac{\mu}{\rho\beta_0 R_\mathrm{eq}^2} T_\mathrm{E} - r h_\mathrm{W} \qquad (21.28)$$

$$\frac{\mathrm{d}T_\mathrm{E}}{\mathrm{d}t} = \left[\mu\left(\gamma \frac{\Delta_h T}{L} + \alpha \frac{\Delta_v T}{H} + \frac{\bar{w} L \Delta_v T}{H^3 g' \rho_0}\right) - r' - \frac{\bar{w}}{H}\right] T_\mathrm{E} + \frac{\bar{w}\Delta_v T}{H^2}\, h_\mathrm{W}. \qquad (21.29)$$

We note the positive temperature feedback in the temperature equation when the coupling parameter μ is large enough. As this term represents the coupling with the atmosphere and the advection feedback, it is clear that it models the amplification process described at the beginning of this section.

With realistic values for the model parameters (coded in `jin.m`), the solution exhibits a damped oscillation (Fig. 21.8; for an animation execute `jinmodel.m`) that models the mechanism depicted in Fig. 21.9. Although this model nicely captures ENSO oscillations with the phase shift between temperature and thermocline-depth anomalies, as well as a period of about 4 years, scientists debate whether ENSO has a natural oscillating cycle as described by the present model or it is triggered by some external effect (e.g., Kessler, 2002).

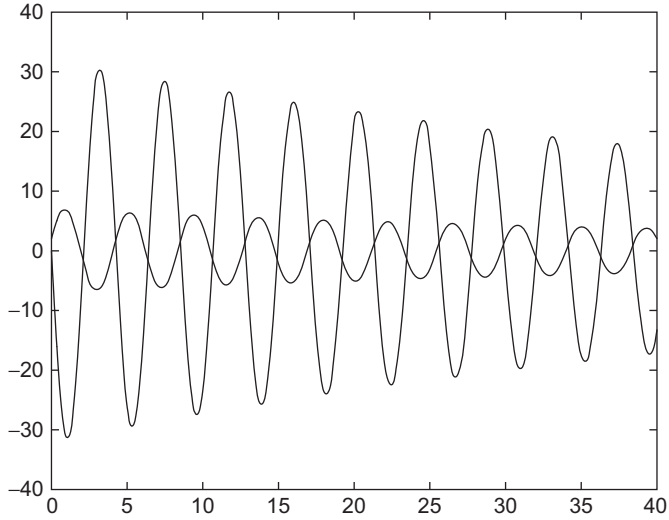

FIGURE 21.8 Temperature anomaly (low amplitude curve) and depth anomaly (high amplitude curve) as a function of time (in years). The period of the slightly damped oscillation is close to 4 years. Scales for temperature and depth are arbitrary.

21.4 ENSO FORECASTING

Forecasting the El Niño–Southern Oscillation (ENSO) event is of great interest to society because an impressive number of its consequences can affect daily life, ranging from changes in weather, appearance of droughts or floodings, to changes in crops, fish catch, and human health. These effects are not only felt in the equatorial region but also in remote locations, such as Australia. Hence, it is no surprise that reliable prediction of an El Niño or La Niña event can be of great help in preparing for the upcoming perturbations.

In forecasting ENSO, monthly averaged weather patterns are of interest because a given month in an El Niño year is quite different from the same month in a La Niña year. But since the forecast has to span several months, if not seasons, sea surface temperature (SST) cannot be considered known, and coupled atmosphere-ocean models are needed. This was recognized by Zebiak and Cane (1987), who succeeded in building the first coupled model to forecast ENSO. The importance of coupling between air and sea can be nicely shown by the following hindcast experiments: The use of observed variations in SST during an ENSO event generally helps to predict the atmospheric part correctly; similarly, using observed variations in atmospheric fluxes along the sea surface reveals the oceanic component of ENSO. Hence, both components are needed for the forecast.

ENSO forecasts differ from weather forecasts in that only average situations are predicted. While weather forecasts are mostly constrained by initial

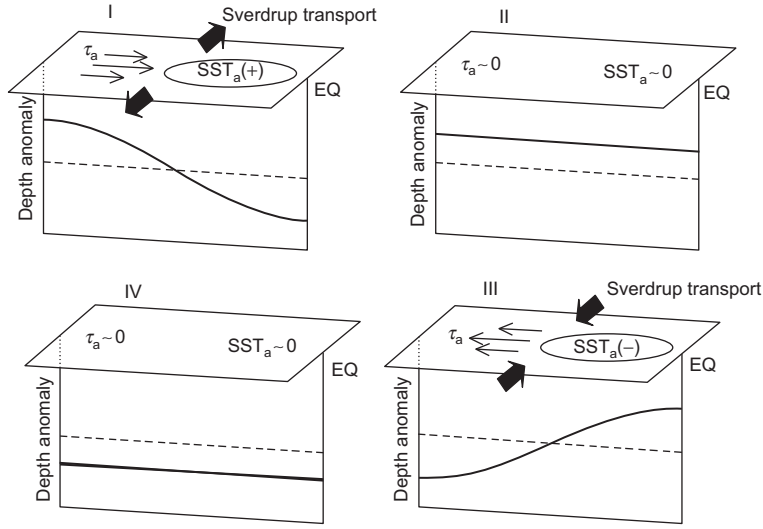

FIGURE 21.9 Discharge/recharge mechanism proposed by Jin (1997a, 1997b) as adapted by Meinen and McPhaden (2000). During a warm, El Niño phase (Phase I), the westerly wind-stress anomaly creates a diverging poleward Sverdrup flow. This removes water from the equatorial Pacific and, via the zonal dynamical balance, the anomalous warm water pool of the eastern Pacific. When the eastern warm water pool no longer exists, no east-west temperature anomaly remains, and the associated anomalous Walker circulation disapears (Phase II). During this stage, winds are those of the climatological Walker circulation, which are responsible for normal upwelling. Since the thermocline is shallower than usual, upwelling in the eastern Pacific brings up colder waters than usual, and the cold, La Niña phase begins. The reversal of the wind-stress anomaly creates an equatorward Sverdrup flow, which recharges the eastern pool (Phase III) until the mean thermocline is deeper than average (Phase IV). At this stage, climatological upwelling again brings up warmer water than usual, and the cycle repeats with a warm phase (Phase I).

conditions in the atmosphere and can be of only short duration, seasonal forecast benefits from the ocean's inertia, and its predictability extends over several months. Hence, seasonal forecast is constrained mostly by initial conditions in the ocean. Observing the tropical ocean is a crucial component of any ENSO forecast system, with the most important data being provided by the Tropical Atmosphere Ocean (TAO) array of moorings and by satellites measuring sea surface height and temperature.

Seasonal forecasting of ENSO is relatively successful because ENSO is known to be the largest single source of predictable internannual variability. Yet, even with a strong signal, models must be able to extract the information amidst the dominant high-frequency signal of atmospheric variability. With unavoidable model uncertainties, this is a challenging task, and one way to reduce uncertainties is to perform model intercomparisons (e.g., Mechoso et al., 1995; Neelin et al., 1992). Models are also used to identify teleconnections that is, correlations between dynamics in distant regions and ENSO events. If such

teleconnections are identified, predictions of El Niño can be "extrapolated" to other regions. The identification of such teleconnections is generally obtained from statistics of model simulations and observations, leading to as many prediction models as identified teleconnections.

Forecasts can also be performed by means of statistics in place of a dynamical model. Empirical predictive models of El Niño begin with past observations of well-chosen parameters and search for correlations by fitting curves across data points, such as a linear regression of the *SOI*. Instead of a priori choosing a functional relationship, self-learning approaches such as neural networks (e.g., Tangang, Tang, Monahan & Hsieh, 1998) or genetic algorithms (e.g., Alvarez, Orfila & Tintore, 2001) select on their own the "best" functions. To do so, data are separated into two sets, a learning and a validation set. From the learning set, the model is given input data called predictors (such as the *SOI* of the previous year) and the known output value called predictand (such as the prediction of *SOI* for the next 6 months). If enough input-output pairs are available, the network or genetic algorithm is able to find a functional relationship that minimizes the error in the output for this given data set. The danger of such an approach is that overfitting may occur: If the functional relationship contains more adjustable parameters than independent data to be fitted, one can always find a "perfect" fit. The latter, however, will work only on this particular data set. An independent validation data set is required on which the model must be tested after the learning phase. If the performance in forecasting degrades significantly after switching from the learning set to the validation set, the model is unreliable. However, if validation is successful, such models offer predictions at extremely small computational costs compared with primitive equation models.

The simplest models, if they have any predictive skill, are therefore valuable in defining base forecasts against which forecats from more complex models may be compared, and to justify their use in operational forecasts, the highly complex dynamical models must demonstrate their superiority in prediction ability compared with statistical models (see Fig. 21.10). At the time of this writing, it appears that dynamical models are better predictors of early stages of an El Niño, but once the event is under way, statistical models are quite satisfactory. The lesson is that the trigger is relatively difficult to identify but that, once an ENSO event begins, it unfolds according to a repeatable pattern.

The search for empirical relationships can of course be guided by physical considerations. For El Niño, wave propagation along the equator and reflection at continental boundaries provide a delayed feedback mechanism on the system. This can be formally translated into a delayed oscillator model (Suarez & Schopf, 1988), the governing equation of which can be expressed in the form:

$$\frac{\mathrm{d}T}{\mathrm{d}t} = aT(t) - aT^3(t) - bT(t-\delta), \tag{21.30}$$

where T stands for a normalized temperature anomaly associated with El Niño, the term aT models the positive feedback of the initial Kelvin wave with the

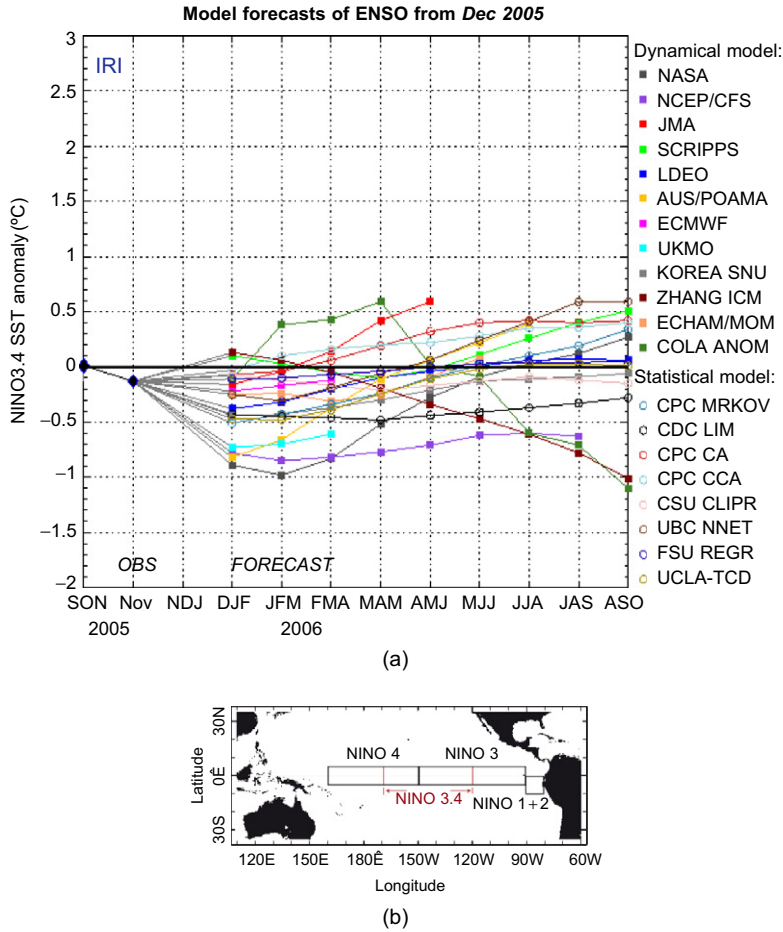

FIGURE 21.10 Prediction of a future El Niño event by means of sea surface temperature (SST) anomaly starting from December 2005 by several models, including coupled ocean-atmosphere primitive equation models and statistical models. Predictions were made for different subregions in a central strip of the basin (see insert), the probablity of El Niño in 2006 was deemed low. (*IRI, International Research Institute for Climate and Society*)

moving atmospheric perturbation, and the cubic term $-aT^3$ represents damping to keep the solution bounded in time.[2] Finally, the last term $-bT(t-\delta)$ is introduced to include the negative feedback of the initial westward Rossby wave that is then reflected as a Kelvin wave of opposite amplitude. The delay δ is readily interpreted in terms of wave travel time along the equator. If the

[2]The temperature T can always be scaled so that the cubic term appears with the same coefficient as the linear feedback.

negative feedback is sufficiently strong, implying a reflection with some degree of amplification, an opposite event can be triggered, and an El Niño may be followed by a La Niña. Parameters of this model can then be fitted to observations if a simple model is desired (Numerical Exercise 21.7).

ANALYTICAL PROBLEMS

21.1. How long does an equatorial Kelvin wave take to cross the entire Pacific Ocean?

21.2. Generalize the equatorial Kelvin-wave theory to the uniformly stratified ocean. Assume inviscid and nonhydrostatic motions. Discuss analogies with internal waves.

21.3. Show that equatorial upwelling (mentioned in Section 15.4; see Fig. 15.6) must be confined at low frequencies to a width on the order of the equatorial radius of deformation.

21.4. In the Indian Ocean, two current-meter moorings placed at the same longitude and symmetrically about the equator ($\pm 1.5^\circ$ of latitude) record velocity oscillations with a dominant period of 12 days. Furthermore, the zonal velocity at the northern mooring leads by a quarter of a period the meridional velocities of both moorings and by half a period the zonal velocity at the southern mooring. The stratification provides $c = 1.2$ m/s. What kind of wave is being observed? What is its zonal wavelength? Can a comparison of the maximum zonal and meridional velocities provide a confirmation of this wavelength?

21.5. Consider geostrophic adjustment in the tropical ocean. What would be the final steady state following the release of buoyant waters with zero potential vorticity along the equator of an infinitely deep and motionless ocean? For simplicity, assume zonal invariance and equatorial symmetry.

21.6. What kind of initial conditions are needed for the delayed oscillator model (21.30)?

21.7. Search for information to check whether the forecast provided in December 2005 of an unlikey El Niño in 2006 came true.

21.8. Show that the linearization of the governing equations for a Kelvin wave is valid as long as the function F is small enough, $|F| \ll 1$.

21.9. Study equatorial upwelling on a beta plane with an arbitrary wind-stress field. Use the approach of Section 8.6 but include a linear friction term in addition to vertical diffusion. What happens to the solution if this linear friction term is dropped? (*Hint*: Do not calculate explicitly the vertical structure of the Ekman layer but integrate vertically.)

NUMERICAL EXERCISES

21.1. Design a numerical solver for the delayed oscillator equation (21.30). Find the solution with $a^{-1} = 50$ days, $\delta = 400$ days, and $b^{-1} = 90$ days for different initial conditions. Then, change to $a^{-1} = 100$ days and $b^{-1} = 180$ days.

21.2. Design a numerical version of the linear reduced-gravity model (21.6), to which a spatially varying zonal wind stress is added, of the form

$$\tau = \tau_0 \mathrm{e}^{-(x^2+y^2)/L^2}. \tag{21.31}$$

Use a finite-difference approach on the Arakawa C-grid and time stepping of your choice. Start with a situation at rest and then apply the wind stress for 30 days. For the wind-stress amplitude and length scale, take $\tau_0 = 0.1$ N/m^2 (directed eastward) and $L = 300$ km. The reduced-gravity model's parameters are $\Delta\rho/\rho_0 = 0.002$ with a thermocline depth $H = 100$ m. For a first simulation, use a closed domain with boundaries at $x = -3000$ km, $x = 10000$ km and $y = \pm 2000$ km. Simulate the evolution for 600 days.

21.3. For the conditions set in Numerical Exercise 21.2 with closed southern and northern boundaries, the perturbation eventually propagates along these boundaries. Which physical process is responsible for this? Modify the southern and northern boundary conditions by opening the domain and apply $v = \pm\sqrt{g'H}\ h$ there. Choose a physically reasonable sign for each boundary by considering a physical interpretation of such boundary conditions.

21.4. Change the topology of the domain in Numerical Exercise 21.3 by adding land points in the southwestern (lower left) and northeastern (upper right) corners to represent continents on each side of the Pacific Ocean and redo the simulations. Can you identify the modes that are now present compared with the symmetric case?

21.5. Search for a spatial discretization of the Coriolis term on the Arakawa C-grid that does not create mechanical work in the sense that, after multiplying the evolution equation for $u_{i-1/2,j}$ by itself and adding a similar product of the $v_{i,j-1/2}$ equation by itself, the Coriolis terms cancel out. (*Hint*: Analyze which products of u and v appear, similar to the analysis of the Arakawa Jacobian performed in Section 16.7 and find how to average by taking into account the variation of y.)

21.6. Using the sea-surface temperature (SST) anomalies and Southern Oscillation Index (SOI) values from 1991 to 2005 included in `soi.m`, perform a linear regression over data windows and find out whether the extrapolation of these regressions is able or unable to predict the SST or SOI at later times. First, use a data window of 4 months and try to extrapolate

for the next month. Plot the prediction error over time when applying the method over all possible data windows. To decide whether the prediction is useful, compare with the prediction error corresponding to simple persistence (constant anomaly). Then, try to change the data window and lead time to improve the prediction. Instead of a linear regression, higher-order polynomial fits may also be tried.

21.7. Do the same as in Numerical Exercise 21.6, but try to calibrate the delayed oscillator model (21.30) for the temperature anomaly. Use the calibrated model for the extrapolation. If necessary, use data windows of several years.

S. George H. Philander
1942–

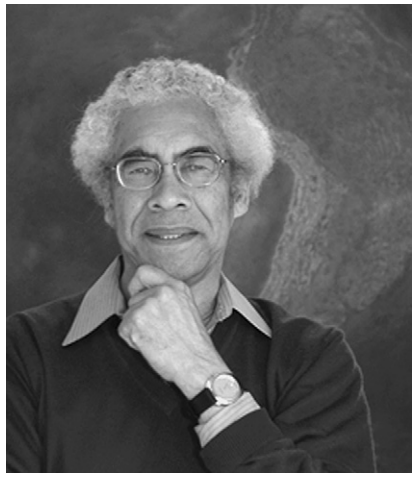

Born in South Africa and son of a poet, George Philander studied applied mathematics and physics before going to Harvard University to obtain his doctorate and embarking on a career in oceanography. His seminal studies of El Niño and, from there, also the Southern Oscillation earned him a position of prominence in Geophysical Fluid Dynamics. From unraveling the global connection between ocean and atmosphere, the study of global warming and climate change necessarily became the next scientific pursuit. Philander is known as a "teacher to his bones," passionate about sharing knowledge with the next generation, and he is praised for his clarity of thought and elegance of expression.

Philander is also a prolific writer, having written multiple books on the subject of El Niño and climate, for both experts and nonexperts alike, including *Our Affair with El Niño – How We Transformed an Enchanting Peruvian Current into a Global Climate Hazard* (2006) an acclaimed book aimed at a broad readership. (*Photo credit: Princeton University*)

Paola Malanotte Rizzoli

Paola Malanotte Rizzoli had obtained a doctorate in quantum mechanics and was well on her way to a distinguished career in physics when a massive flood of Venice, where she worked at the time, made her change her mind. She switched to physical oceanography and obtained a second doctorate. Her contributions to this field have been significant and varied, spanning the theory of long-lived geophysical structures, such as eddies and hurricanes, numerical modeling of the Atlantic Ocean and Gulf Stream system, the Black Sea ecosystem, data assimilation, and tropical-subtropical interactions.

Professor Rizzoli teaches at the Massachusetts Institute of Technology and lectures across the world. She is known as a dynamic speaker and an inspiring scientist. In addition to her teaching and research, she has served the oceanographic community in a number of capacities, at both national and international levels.

Never abandoning her love for Venice, Paola Rizzoli was instrumental in developing a system of sea gates to protect the city from future floods and sea level rise. This protection system is currently under construction. (*Photo MIT archives*)